ISSN 0021-3640, JETP Letters, 2025, Vol. 122, No. 1, pp. 1–7. © The Author(s), 2025. This article is an open access publication.
Russian Text © The Author(s), 2025, published in Pis'ma v Zhurnal Eksperimental'noi i Teoreticheskoi Fiziki, 2025, Vol. 122, No. 1, pp. 3–9.

FIELDS, PARTICLES, AND NUCLEI

Search for Large Extra Dimensions in the DANSS Experiment

I. G. Alekseev[a,b,c,d], V. V. Belov[d,e], A. D. Bystryakov[b,e,f], P. A. Gorovtsov[c], M. V. Danilov[b,d], I. V. Zhitnikov[d,e], D. R. Zinatulina[e,g], S. V. Kazartsev[d,e], A. S. Kobyakin[a,b,c], A. L. Krapiva[a,b,c], A. S. Kuznetsov[e], I. V. Machikhil'yan[h], N. A. Mashin[a,b,c], D. V. Medvedev[e], V. M. Nesterov[a,b], D. V. Ponomarev[b,d,e], V. Yu. Rusinov[a,b], E. I. Samigullin[a,b], D. N. Svirida[a,b,d], N. A. Skrobova[a,b,d,*], E. I. Tarkovskii[a], D. V. Filosofov[e], M. V. Fomina[e], E. A. Shevchik[e], M. V. Shirchenko[d,e], Yu. A. Shitov[i], and E. A. Yakushev[e]

[a] *National Research Center Kurchatov Institute, Moscow, 123182 Russia*
[b] *Lebedev Physical Institute, Russian Academy of Sciences, Moscow, 119991 Russia*
[c] *Moscow Institute of Physics and Technology (National Research University), Dolgoprudny, Moscow region, 141701 Russia*
[d] *Institute for Nuclear Research, Russian Academy of Sciences, Moscow, 117312 Russia*
[e] *Joint Institute for Nuclear Research, Dubna, Moscow region, 141701 Russia*
[f] *Dubna State University, Dubna, Moscow region, 141982 Russia*
[g] *Voronezh State University, Voronezh, 394018 Russia*
[h] *Dukhov Automatics Research Institute, Moscow, 127055 Russia*
[i] *Institute of Experimental and Applied Physics, Czech Technical University in Prague, Husova 240/5, 110 00 Prague, Czech Republic*
* *e-mail: skrobovana@lebedev.ru*

Received April 2, 2025; revised May 20, 2025; accepted May 22, 2025

The DANSS detector is located near the power reactor at the Kalinin Nuclear Power Plant (at distances of 10.9–12.9 m) and is able to detect up to 5000 antineutrino events per day. The results of the search for Large Extra Dimensions in the simplest case of a single dominant large extra dimension are discussed. The particle oscillations to a finite-size extra dimension are assumed in this theory, and its predictions depend on the difference between the squared masses, as well as on the absolute scale of the neutrino masses. The sensitivity of the experiment to Large Extra Dimensions for various values of the model parameters such as the size of the large extra dimension a and the lightest-neutrino mass m_0 can be determined by its Monte Carlo simulation. No statistically significant indications of the existence of Large Extra Dimensions have been obtained from the analysis of almost 5.8 million antineutrino events (the statistical confidence of the best point is only 2.0σ (1.8σ) for the normal (inverted) ordering of neutrino masses). The bounds have been determined for the size of the extra dimension and the lightest neutrino mass. These bounds for a number of regions are the best in the world. These bounds exclude a large fraction of the parameters preferable for explaining the gallium anomaly and the reactor antineutrino anomaly in this model, including the corresponding best points.

DOI: 10.1134/S0021364025607110

1. INTRODUCTION

Neutrino physics is currently one of the most fascinating branches of particle physics. It contains many unsolved mysteries, among which are neutrino oscillations. The three-generation model with massive neutrinos describes experimental data with an outstanding accuracy, but nevertheless, some anomalies are still observed, e.g., the so-called reactor antineutrino anomaly (RAA), which consists in a lack of reactor antineutrino flux [1], and the gallium anomaly (GA), which consists in a lack of neutrino events in the calibration measurements using radioactive sources in the SAGE and GALLEX experiments [2–6]. The GA was confirmed with a confidence of more than 5σ in the BEST experiment [7, 8]. The RAA is most likely caused by an overestimation of the contribution to the antineutrino spectra from fission products [9]; however, it is too early to draw a final conclusion. Various hypotheses have been proposed to explain the RAA and GA, including the existence of a sterile neutrino or Large Extra Dimensions (LED). This work is devoted to the search for the LED conducted in the context of the LED model with a single dominant large extra dimension.

2. LED MODEL

The LED model was proposed to solve the gauge hierarchy problem, i.e., the problem of the large dif-

ference between the energy scales of the electroweak ($M_W \sim 80$ GeV) and gravitational ($M_{Pl} \sim 2 \times 10^{18}$ GeV) interactions. It is assumed that the observed space–time with 3 + 1 dimensions exists on a brane embedded in a space with a larger dimension, while the remaining dimensions are compactified at scale a usually not exceeding a few microns [10, 11]. The Newton's law should be considered in this theory in different ways depending on the distance between gravitating objects. Here we present a qualitative reasoning for the case of n extra dimensions. The space is effectively flat at small scales ($r \ll a$) and has a dimension of $3 + n$; therefore, the gravitational potential is written as

$$V(r) \sim \frac{m_1 m_2}{M_{Pl(4+n)}^{n+2}} \frac{1}{r^{n+1}}, \quad r \ll a. \tag{1}$$

At a large scale $r \gg a$, $V(r)$ is presented by the usual expression, in which the Planck mass is renormalized by introducing an extra dimension [10]:

$$V(r) \sim \frac{m_1 m_2}{M_{Pl(4+n)}^{n+2} a^n} \frac{1}{r}, \quad r \gg a. \tag{2}$$

This approach is applicable only for extra dimensions of a sufficiently small size, since the gravitational forces have been directly measured up to distances of $r \sim 1$ mm [12]. In the case of a single extra dimension, renormalization of the Planck mass to a scale of 1 TeV requires that an extra dimension with the size of approximately the Solar System be introduced, which is excluded by gravity measurements (see the review in [13]). Therefore, theories with $n \geq 2$ extra dimensions are usually considered.

The LED model can also explain the lack of (anti)neutrinos in the (RAA) GA. In this paper, we discuss the case of one dominant large extra dimension. The sizes of the remaining dimensions are much smaller than the larger one, and the neutrino oscillations in them can be ignored. In this model, the right-handed neutrinos $\nu_{R,e}$ (and $\bar{\nu}_{L,e}$) can be captured in this extra dimension, where they form the so-called Kaluza–Klein tower. Moreover, in this mechanism, due to the small volume of the LED, the coupling constant between the right- and left-handed neutrinos is suppressed, which leads to small neutrino masses [14]. Under the assumption that $am_i \ll 1$, the survival amplitude of the electron antineutrino is [15]:

$$A_{ee} = \sum_{i=1,2,3} |U_{ei}|^2 A_i, \tag{3}$$

where U_{ei} are the elements of the PMNS neutrino mixing matrix [13], and A_i are the mass state amplitudes given by the relationship

$$A_i = \left(1 - \frac{\pi^2}{6} m_i^2 a^2\right)^2 \exp\left(i \frac{m_i^2 L}{2E}\right) + 2m_i^2 \exp\left(i \frac{m_i^2 L}{E}\right) \sum_{n=1}^{\infty} \frac{\exp\left(i \frac{(m_n^{KK})^2 L}{2E}\right)}{(m_n^{KK})^2}, \tag{4}$$

where m_i is the mass of the ith neutrino state (where i is the subscript, which numbers the neutrino states; otherwise, it is an imaginary unit), a is the size of the extra dimension, L is the distance between the points of antineutrino production and detection, E is the antineutrino energy, and $m_n^{KK} = \frac{n}{a}$ is the masses of the states in the Kaluza–Klein tower, the eigenstates in the extra dimension that are plane waves. It is important to note the series $\sum \frac{\exp(ixn^2)}{n^2}$ in the second term, where $x = \frac{L}{2Ea^2}$. It converges absolutely, as it is majored by a series of inverse squares $\sum \frac{1}{n^2}$. Nevertheless, its term-by-term derivative $\sum i \exp(in^2 x)$ may diverge, which means that this term in A_i can rapidly oscillate.

The first parameter of the theory is the size a of the extra dimension. The neutrino masses enter into Eq. (4) so that the total amplitude A_{ee} depends on the differences between the squared masses, as well as on the absolute value of the lightest-neutrino mass m_0, which serves as the second parameter. As a result, the total amplitude is also sensitive to the neutrino mass ordering. Figure 1 shows the dependence of the absolute value of the amplitudes A_i on m_0 at $L = 12.89$ m, $E_\nu = 4$ MeV, and $a = 0.5$ μm. The amplitudes A_1 and A_2 are basically higher than A_3. Since they appear in Eq. (3) for the probability of survival with larger weights ($|U_{e1}| \sim 0.8$, $|U_{e2}| \sim 0.5$, $|U_{e3}| \sim 0.1$, [13]), it turns out that, at equal values of the LED parameters, the survival probability is on average higher for the normal ordering of neutrino masses and, hence, the sensitivity to oscillations into extra dimensions is lower.

3. DANSS EXPERIMENT

The DANSS experimental setup [16] is located near the reactor core at the Kalinin Nuclear Power Plant (KNPP) at a distance of ≈11 m from the reactor core center. The sensitive volume of the DANSS detector consists of 2500 strips made of a plastic scintillator measuring $100 \times 4 \times 1$ cm^3. The signal is read out from the strips using three wavelength-shifting fibers glued by a two-component optical gel into the longitudinal grooves milled in the strips. The light from the central fiber is detected by a silicon photo-

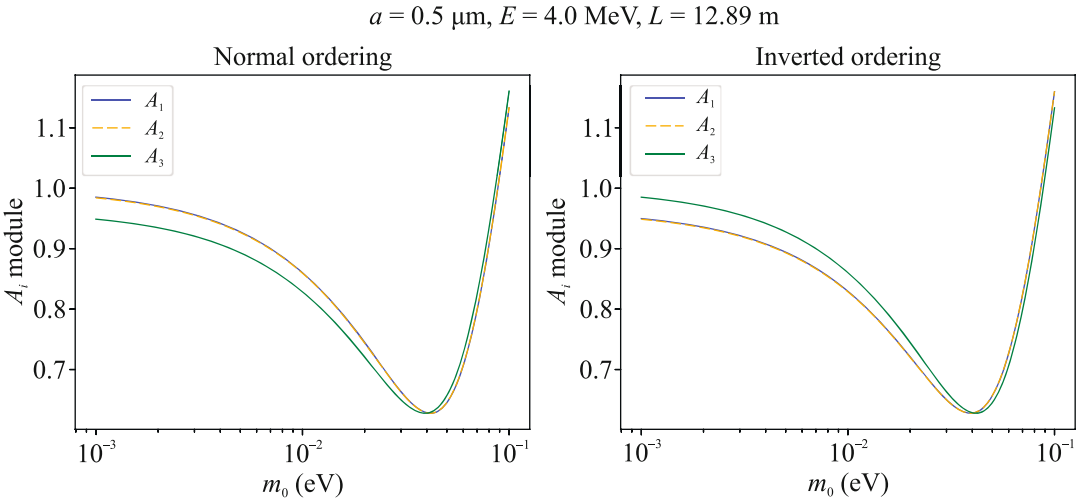

Fig. 1. (Color online) Absolute values of the amplitudes (4) versus the mass of the lightest neutrino m_0 for $L = 12.89$ m, $E_\nu = 4$ MeV, and $a = 0.5$ μm for the (left) normal and (right) inverted neutrino mass ordering. The amplitudes A_1 and A_2 are almost indistinguishable, since the square of the mass difference Δm^2_{21} is much smaller than Δm^2_{32}.

multiplier (SiPM). The side fibers form a pair and are coupled to a photomultiplier tube (PMT). Each PMT reads the signal from a group of 50 strips. A reflective coating containing gadolinium is applied to the surface of the strips to capture neutrons generated in the inverse beta decay (IBD) reaction

$$\bar{\nu}_e + p \to n + e^+. \tag{5}$$

The strips are stacked in 100 layers in height, each with 25 pieces. The strips of adjacent layers are laid in perpendicular directions, thus providing reconstruction of the three-dimensional event structure from two projections onto two side surfaces. The sensitive volume is surrounded by the passive shielding consisting of copper, lead, and borated polyethylene layers, as well as by a veto system consisting of scintillation counters [16]. The detector is fixed in place on a movable platform used to change the detector-to-reactor distance. The data were acquired in three positions: *Top* with $L_t = 10.89$ m, *Middle* with $L_m = 11.88$ m, and *Bottom* with $L_b = 12.86$ m, where L is the distance between the reactor and detector centers. In this paper, we considered the data collected in the *Top* and *Bottom* positions with a total number of events slightly less than 5.8 million.

Reactor antineutrinos are detected in the IBD reaction: $\bar{\nu}_e + p \to n + e^+$. An antineutrino event is considered to be the coincidence of a prompt signal from a positron e^+ and a signal delayed for a time in the range 1–50 μs from a neutron capture by Gd. The neutron capture is detected by a burst of γ rays with a total energy of ~8 MeV. As a first approximation, we can assume that the positron energy is $E_{e^+} \approx E_{\bar{\nu}_e} - 1.8$ MeV; nevertheless, a response matrix was simulated for data analysis [17, 18] using the Geant4 software [19]. It represented the relationship between the antineutrino energy spectrum and the detected positron spectrum. The ratio of the signal events to the correlated background events achieved using the event selection criteria exceeded 50 in the positron energy range of 1.5–7 MeV. The background due to random coincidences of the prompt and delayed signals was measured with a high accuracy directly in the experiment and was subtracted without increasing the measurement errors [20]. The latest results of the DANSS experiment on the search for sterile neutrinos were presented in [20].

4. SIMULATION OF THE EXPECTED SIGNAL

The Monte Carlo (MC) simulation is used to calculate the predicted antineutrino spectra for different values of the LED parameters. The production points of antineutrinos in the reactor $\mathbf{r}_r$ and their detection points $\mathbf{r}_d$ are generated randomly. The reactor model is a cylinder with height $h = 3.7$ m, a diameter of 3.2 m, and a known spatial distribution of fission points. The detection points are uniformly distributed over the confidence volume of the detector, which has a cubic shape with a side of 92 cm. The central axes of the detector and reactor coincide. The probability that $\bar{\nu}_e$ with the energy E produced in $\mathbf{r}_r$ has interacted in $\mathbf{r}_d$ is

$$\begin{aligned} dP_{ee} &= \left|A_{ee}(a, m_0, E, L)\right|^2 \times profile(\mathbf{r}_r) \\ &\times HM(E)dE \times \frac{1}{L^2} d^3\mathbf{r}_r d^3\mathbf{r}_d, \end{aligned} \tag{6}$$

where A_{ee} is the amplitude calculated by Eq. (3), L is the distance traveled by $\bar{\nu}_e$, *profile* denotes the distri-

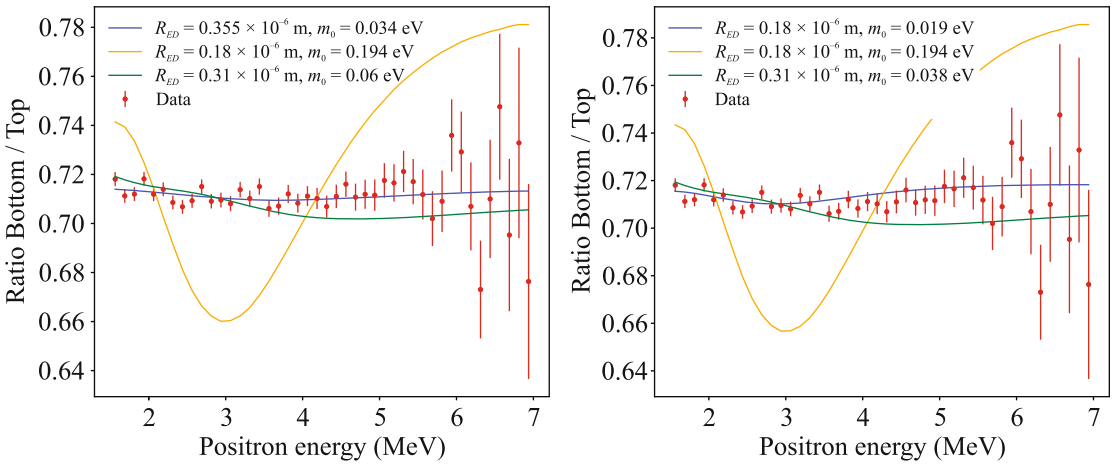

Fig. 2. (Color online) Ratios of the positron energy spectra obtained in the Monte Carlo simulation, for the best points of fits for the (blue line) DANSS, (orange line) GA, and (green line) RAA data for the (left panel) normal and (right panel) inverted ordering. The red points with error bars indicate the ratio of the experimental spectra.

bution of fission points inside the reactor (provided by the KNPP personnel), *HM* denotes the Huber–Muller model and describes the energy spectrum of $\bar{\nu}_e$ generated in the reactor [21, 22], and $\frac{1}{L^2}$ is the term describing the geometric attenuation of the antineutrino flux. The ratio of the positron spectra in the *Bottom* and *Top* positions is used in this analysis, so that the systematic uncertainty caused by the selection of a specific antineutrino spectrum model is strongly suppressed. It has been verified that, when the Huber–Muller and Daya Bay (DB) spectra [23] are used, the difference in the results is negligible and significantly smaller than when the parameters of other systematic uncertainties are varied. Antineutrinos are simulated in the energy range from the reaction threshold (5) of 1.8 to 9.6 MeV for the *Top* and *Bottom* detector positions. In the next step, the $\bar{\nu}_e$ energy spectra obtained thereby are convoluted with the previously simulated response matrix and the positron spectra are obtained. Finally, the positron spectra are cut at values from 1.5 to 7 MeV. The influence of the correlated background increases for the low-energy part of the spectrum, since the uncertainties in it increase at low positron energies, and statistical errors are large for the high-energy part. In what follows, the spectra are always understood as the positron spectra unless otherwise is specified. Examples of the obtained spectrum ratios are shown in Fig. 2. In the space of the LED-model parameters, they correspond to the best point of the DANSS fit and the best points of the RAA and GA data fits [24]. Antineutrinos were generated on a grid in the LED-model parameter space 60 × 60 in size.

5. DATA ANALYSIS

The null hypothesis was tested at the beginning of the LED-searching analysis. This hypothesis corresponds to the absence of extra dimensions and, therefore, the absence of oscillations in them. Since the normal oscillations in the three-generation model can be ignored at $\bar{\nu}_e$ energies of ~3–9 MeV and reactor-to-detector distances of ~11–13 m, the null hypothesis predicts an almost constant energy ratio of the spectra. A very small deviation from the constant is possible due to the contribution of the background. Of course, a low (~2%) correlated background, which is practically independent of the detector position, is subtracted from the measured IBD positron spectra. However, it can vary within its uncertainty during χ^2 minimization; see Eq. (6). The Asimov dataset was compiled based on the null hypothesis prediction for the spectra and the available experimental data errors and was used thereafter to determine the DANSS sensitivity to antineutrino oscillations into extra dimensions similarly to the algorithm for determining the sensitivity to oscillations into the sterile neutrino state [25].

The experimental data were analyzed using the χ^2 statistics obtained by the formula

$$\chi^2 = \sum_{i\in \text{bins}} \frac{\left(R_{i,MC}(\eta_j)k - R_{i,\text{data}}\right)^2}{\sigma_i^2} + \sum_j \frac{(\eta_j - \eta_{0,j})^2}{\sigma_{\eta_j}^2}, \quad (7)$$

where R_i is the ratio of the MC spectra or the experimental data with error σ_i, and η_j are the parameters of systematic uncertainties with nominal $\eta_{0,j}$ values and errors σ_{η_j}. The following systematic uncertainties were taken into account [26]: the detector efficiency ratio at the *Bottom* and *Top* positions k, the uncertainty in the

Table 1. Systematic uncertainties taken into account. Their detailed description is given in the text

η	*k*	*b*	K_E	*smear*	*shift*, keV	*move*, cm
η_0	1	0	1	0	0	0
σ_η	4×10^{-3}	7×10^{-3}	0.02	$\frac{6\%}{\sqrt{E}} + 2\%$	50	5

background subtracted from the experimentally measured spectra *b*, the calibration coefficient of the energy scale K_E, the additional smearing of the MC energy spectra *smear*, the shift of the energy scale in the MC simulation relative to the experiment *shift*, and the detector displacement along the vertical axis *move*. The nominal values and errors of the systematic uncertainties are given in Table 1. The background-level deviation of 1σ corresponds to 7×10^{-3} of the signal events per day in the *Top* detector position. The K_E, *smear*, and *shift* values are taken into account using various response matrices simulated in the Geant4 software with the corresponding changes in the detector model. For the *move* value to be taken into account, the initial antineutrino spectra were simulated for a detector shifted up and down by 5 cm. This has made it possible to obtain numerical derivatives for the spectra with respect to these parameters.

6. RESULTS AND DISCUSSION

We analyzed almost 5.8 million antineutrino events in the positron energy range of 1.5–7 MeV acquired from October 2016 to January 2024. The DANSS sensitivity to $\bar{\nu}_e$ oscillations into extra dimensions and the contours of exclusion regions are shown in Fig. 3. The null hypothesis describes the experimental data with $\chi^2/\mathrm{NDF} = 36/44$. The contours represent the boundaries of the sensitivity and exclusion regions at 90 and 99% C.L.; they were obtained by comparing the ratios of MC spectra and experimental data using Wilks' theorem. In this case, the test statistics $\Delta\chi^2 = \chi^2 - \chi^2_{\min}$ is considered. The statistical confidence levels of 90 and 99% for two degrees of freedom correspond to $\Delta\chi^2 = 4.61$ and 6.18, respectively [27]. It is assumed for open contours that the regions located above and to the right (i.e., large parameter values) are excluded. The best point of the DANSS fit lies between the sensitivity contours at 90 and 99% C.L. for both hierarchies. Its coordinates in the parameter space of the theory are $a = 0.335$ μm and $m_0 = 0.034$ eV ($a = 0.180$ μm and $m_0 = 0.017$ eV) for the normal (inverted) ordering. The confidence level of the best point was 2.0σ and 1.8σ for the normal and inverted ordering, respectively. Thus, no statistically significant confirmation of reactor antineutrino oscillations into extra dimensions has been detected.

Figure 4 shows the exclusion contours obtained from the DANSS data in comparison with the contours obtained using the gallium experiment data (GA) in [24], on the reactor antineutrino fluxes (RAA), and analysis [24] of the Daya Bay [28] and MINOS [29] data. A large part of the LED parameter space allowed by GA and RAA data analysis is excluded by DANSS with more than 99% C.L. The

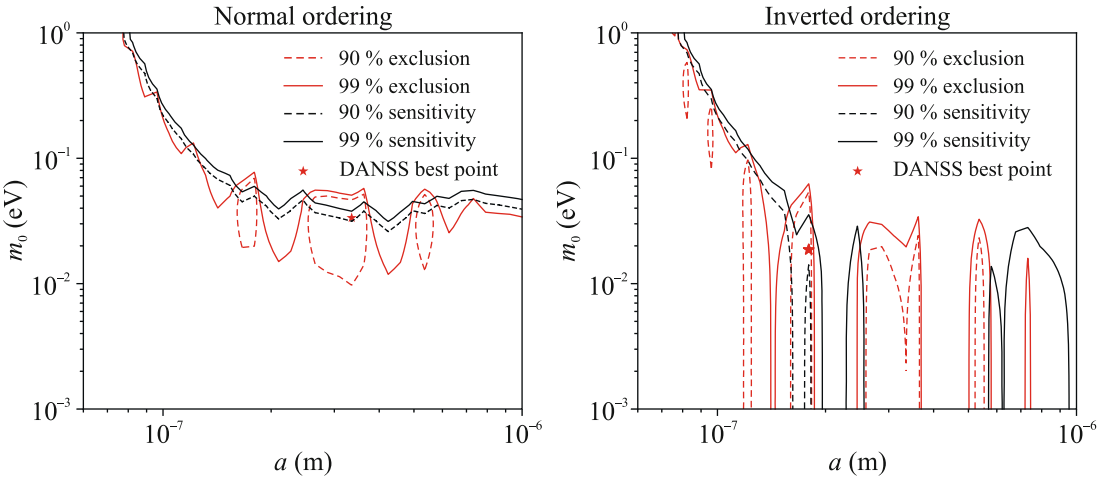

Fig. 3. (Color online) (Black lines) Sensitivity and (red lines) exclusion contours in the LED-model parameter region, which correspond to the (dashed lines) 90 and (solid lines) 99% C.L.

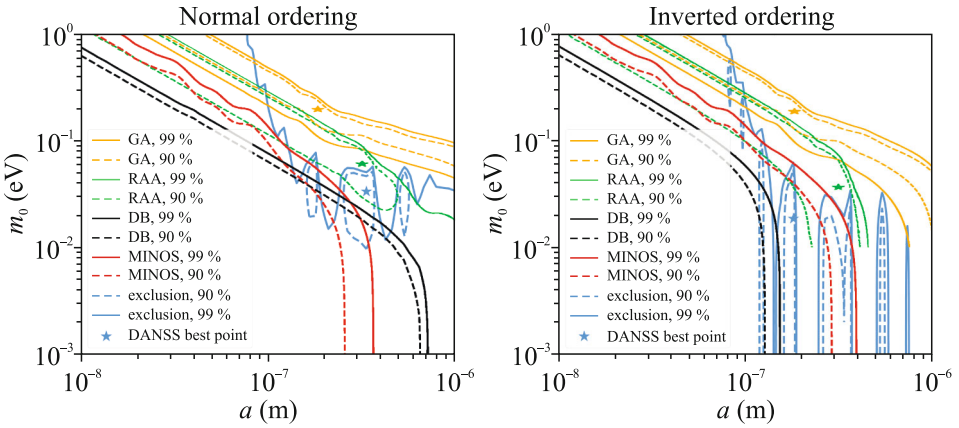

Fig. 4. (Color online) Exclusion contours obtained from the (blue lines) DANSS, (black lines) DB, and (red lines) MINOS data, as well as confidence intervals of preferred parameters determined from the (orange lines) GA and (green lines) RAA data, for (dashed lines) 90 and (solid lines) 99% C.L. The best points of the DB fit for both hierarchies are located outside the investigated part of the parameter space, namely, in the region of smaller a values.

best fit points of RAA and GA are excluded by DANSS with a confidence of 4.2σ and more than 5σ, respectively, for both hierarchies. For a number of regions, the obtained bounds on the extra-dimension size and the lightest-neutrino mass are the best in the world. The exclusion contours determined by DANSS are in agreement with the Daya Bay exclusions obtained using model-dependent additional information on the absolute counts of neutrino events. For the normal hierarchy, the contours obtained from the MINOS data are also consistent with the DANSS result, covering a slightly larger part of the a region and low m_0 values, whereas for the inverted hierarchy, the region of parameters excluded by the MINOS data is completely embedded in the region excluded by the Daya Bay data.

ACKNOWLEDGMENTS

We are grateful to the administration and Radiation Safety Department of the Kalinin Nuclear Power Plant for their constant support and assistance during the experiment.

FUNDING

This work was supported by the Ministry of Science and Higher Education of the Russian Federation (project no. 075-15-2024-541, State Science Project).

CONFLICT OF INTEREST

The authors of this work declare that they have no conflicts of interest.

OPEN ACCESS

REFERENCES

1. G. Mention, M. Fechner, Th. Lasserre, Th. A. Mueller, D. Lhuillier, M. Cribier, and A. Letourneau. Phys. Rev. D **83**, 073006 (2011). https://doi.org/10.1103/PhysRevD.83.073006
2. J. N. Abdurashitov, V. N. Gavrin, S. V. Girin, et al. (SAGE Collab.), Phys. Rev. C **59**, 2246 (1999). https://doi.org/10.1103/PhysRevC.59.2246
3. J. N. Abdurashitov, V. N. Gavrin, S. V. Girin, et al. (SAGE Collab.), Phys. Rev. C **73**, 045805 (2006). https://doi.org/10.1103/PhysRevC.73.045805
4. W. Hampel, G. Heusser, J. Kiko, et al. (GALLEX Collab.), Phys. Lett. B **420**, 114 (1998). https://doi.org/10.1016/S0370-2693(97)01562-1
5. F. Kaether, W. Hampel, G. Heusser, J. Kiko, and T. Kirsten, Phys. Rev. B **685**, 47 (2010). https://doi.org/10.1016/j.physletb.2010.01.030
6. M. Laveder, Nucl. Phys. B Proc. Suppl. **168**, 344 (2007). https://doi.org/10.1016/j.nuclphysbps.2007.02.037

7. V. V. Barinov, B. T. Cleveland, S. N. Danshin, et al. (BEST Collab.), Phys. Rev. Lett. **128**, 232501 (2022). https://doi.org/10.1103/PhysRevLett.128.232501
8. V. V. Barinov, S. N. Danshin, V. N. Gavrin, et al. (BEST Collab.), Phys. Rev. C **105**, 065502 (2022). https://doi.org/10.1103/PhysRevC.105.065502
9. V. Kopeikin, M. Skorokhvatov, and O. Titov, Phys. Rev. D **104**, L071301 (2021). https://doi.org/10.1103/PhysRevD.104.L071301
10. N. Arkani-Hamed, S. Dimopoulos, and G. R. Dvali, Phys. Lett. B **429**, 263 (1998); arXiv: hep-ph/9803315. https://doi.org/10.1016/S0370-2693(98)00466-3
11. H. Davoudiasl, P. Langacker, and M. Perelstein, Phys. Rev. D **65**, 105015 (2002); arXiv: hep-ph/0201128. https://doi.org/10.1103/PhysRevD.65.105015
12. D. J. Kapner, T. S. Cook, E. G. Adelberger, J. H. Gundlach, B. R. Heckel, C. D. Hoyle, and H. E. Swanson, Phys. Rev. Lett. **98**, 021101 (2007); arXiv: hep-ph/0611184. https://doi.org/10.1103/PhysRevLett.98.021101
13. P. A. Zyla, R. M. Barnett, J. Beringer, et al. (Part. Data Group), Phys. Rev. D **110**, 030001 (2024). https://doi.org/10.1103/PhysRevD.110.030001
14. N. Arkani-Hamed, S. Dimopoulos, G. R. Dvali, and J. March-Russell, Phys. Rev. D **65**, 024032 (2001); arXiv: hep-ph/9811448. https://doi.org/10.1103/PhysRevD.65.024032
15. P. A. N. Machado, H. Nunokawa, F. A. Pereirados Santos, and R. Zukanovich Funchal, arXiv: 1110.1465 [hep-ph] (2011).
16. I. Alekseev, V. Belov, V. Brudanin, et al. (DANSS Collab.), J. Instrum. **11**, 11011 (2016); arXiv: 1606.02896[physics.ins-det]. https://doi.org/10.1088/1748-0221/11/11/P11011
17. I. Alekseev, V. Belov, V. Brudanin, et al. (DANSS Collab.), Phys. Lett. B **787** (10), 56 (2018). https://doi.org/10.1016/j.physletb.2018.10.038
18. D. Svirida, J. Phys.: Conf. Ser. **1690**, 012179 (2020). https://doi.org/10.1088/1742-6596/1690/1/012179
19. S. Agostinelli, J. Allison, K. Amako, et al., Nucl. Instrum. Methods Phys. Res., Sect. A **506**, 250 (2003). https://doi.org/10.1016/S0168-9002(03)01368-8
20. I. G. Alekseev, Bull. Lebedev Phys. Inst. **51**, 8 (2024). https://doi.org/10.3103/S1068335623601796
21. P. Huber, Phys. Rev. C **84**, 024617 (2011). https://doi.org/10.1103/PhysRevC.84.024617
22. Th. A. Mueller, D. Lhuillier, M. Fallot, A. Letourneau, S. Cormon, M. Fechner, L. Giot, T. Lasserre, J. Martino, G. Mention, A. Porta, and F. Yermia, Phys. Rev. C **83**, 054615 (2011). https://doi.org/10.1103/PhysRevC.83.054615
23. F. P. An, A. B. Balantekin, M. Bishai, et al. (Daya Bay Collab.), Chin. Phys. C **45**, 073001 (2021). https://doi.org/10.1088/1674-1137/abfc38
24. D. V. Forero, C. Giunti, C. A. Ternes, and O. Tyagi, Phys. Rev. D **106**, 035027 (2022); arXiv: 2207.02790 [hep-ph]. https://doi.org/10.1103/PhysRevD.106.035027
25. N. A. Skrobova, Bull. Lebedev Phys. Inst. **47**, 101 (2020). https://doi.org/10.3103/S1068335620040077
26. N. A. Skrobova, Bull. Lebedev Phys. Inst. **47**, 271 (2020). https://doi.org/10.3103/S1068335620090067
27. S. S. Wilks, Ann. Math. Stat. **9**, 60 (1938). https://doi.org/10.1214/aoms/1177732360
28. D. Adey, F. P. An, A. B. Balantekin, et al. (Daya Bay Collab.), Phys. Rev. Lett. **121**, 241805 (2018). https://doi.org/10.1103/PhysRevLett.121.241805
29. P. Adamson, I. Anghel, A. Aurisano, et al. (MINOS Collab.), Phys. Rev. D **94**, 111101 (2016). https://doi.org/10.1103/PhysRevD.94.111101

Translated by N. Goryacheva